Fermilab FERMILAB-Pub-00/099-E E835 May 2000

May 9, 2000

Measurement of the branching ratios $\psi' \to e^+ e^-$, $\psi' \to J/\psi\,\pi^0\,\pi^0$ and $\psi' \to J/\psi\,\eta$

The Fermilab E835 Collaboration

M.Ambrogiani[2], S.Bagnasco[3], W.Baldini[2], D.Bettoni[2], G.Borreani[6], A.Buzzo[3], R.Calabrese[2], M.Cardarelli[3], R.Cester[6], P.Dalpiaz[2], I.Dobbs-Dixon[4], X.Fan[5], G.Garzoglio[1], K.Gollwitzer[4], A.Hahn[1], S.Jin[5], J.Kasper[5], G.Lasio[5], M.Lo Vetere[3], E.Luppi[2], P.Maas[5], M.Macrì[3], M.Mandelkern[4], F.Marchetto[6], M.Marinelli[3], W.Marsh[1], M.Martini[2], E.Menichetti[6], R.Mussa[2], M.M.Obertino[6], M.Pallavicini[3], N.Pastrone[6], C.Patrignani[3], T.K.Pedlar[5], J.Peoples Jr.[1], S.Pordes[1], E.Robutti[3], J.Rosen[5], P.Rumerio[6], A.Santroni[3], M.Savrié[2], J.Schultz[4], K.K.Seth[5], G.Stancari[2], M.Stancari[4], J.Streets[1], A.Tomaradze[5], S.Werkema[1] and G.Zioulas[4]

[1] *Fermi National Accelerator Laboratory, Batavia, Illinois 60510*
[2] *Istituto Nazionale di Fisica Nucleare and University of Ferrara, 44100 Ferrara, Italy*
[3] *Istituto Nazionale di Fisica Nucleare and University of Genova, 16146 Genova, Italy*
[4] *University of California at Irvine, California 92697*
[5] *Northwestern University, Evanston, Illinois 60208*
[6] *Istituto Nazionale di Fisica Nucleare and University of Torino, 10125 Torino, Italy*

Abstract

We have determined the following ψ' branching ratios using the large event sample collected by Fermilab experiment E835 in the reaction $p\bar{p} \to \psi'$: $\mathcal{B}(\psi' \to e^+e^-) = (7.4 \pm 0.2 \pm 0.7) \times 10^{-3}$, $\mathcal{B}(\psi' \to J/\psi\,\pi^0\,\pi^0) = (18.7{\pm}0.9{\pm}1.3)\%$ and $\mathcal{B}(\psi' \to J/\psi\,\eta) = (4.1{\pm}0.3{\pm}0.5)\%$.

PACS number(s): 13.75.Cs, 14.40.Gx, 13.25.Gv, 13.20.Gd

1 Introduction

The ψ' branching ratios have been measured in a number of experiments in e^+e^- collisions [1]; some branching ratios, namely that for e^+e^- and those for final states including J/ψ, have been measured in $p\bar{p}$ annihilations by Fermilab experiment E760 with comparable or better precision [2].

Fermilab experiment E835, an upgrade and continuation of experiment E760, took data during the Fermilab fixed target run in 1996 and 1997. The ψ' sample collected by E835, based on 10.07 pb^{-1}, is nearly 5 times larger than that of E760. The greater integrated luminosity and upgrades to the detector allow us to improve our branching ratio measurements for the following ψ' decays:

$$\psi' \longrightarrow e^+e^- \quad (1)$$
$$\psi' \longrightarrow J/\psi\,\pi^0\,\pi^0 \quad (2)$$
$$\psi' \longrightarrow J/\psi\,\eta \quad (3)$$

We outline the experimental technique in section 2; section 3 describes the experimental setup, with emphasis on the features that are relevant for this analysis; a detailed description of the event selection is presented in section 4; the efficiency and acceptance calculations are discussed in section 5. In section 6 we summarize our results and compare them with prior results.

2 Experimental technique

Our determination of the ψ' branching ratios follows the method adopted by our previous experiment E760 [2] and recalled here. Charmonium states are studied in $\bar{p}p$ annihilations in which all charmonium states can be formed. The signal is extracted from the huge non-resonant hadronic background by selecting charmonium decays to electromagnetic final states. The required high luminosity is achieved by using a H_2 molecular cluster jet target [3] intersecting the coasting antiproton beam in the Fermilab Antiproton Accumulator.

Decays of the ψ' are studied by observing the reactions

$$p\bar{p} \longrightarrow \psi' \longrightarrow e^+e^- \quad (4)$$
$$p\bar{p} \longrightarrow \psi' \longrightarrow J/\psi + X \longrightarrow e^+e^- + X \quad (5)$$

by identifying events with an e^+e^- pair of large invariant mass. Candidates are kinematically analyzed to determine whether they are consistent with decay modes (1), (2) and (3).

The number $N_{\rm mode}$ of events collected for a decay mode is given by

$$N_{\rm mode} = \mathcal{B}(\psi' \to {\rm mode})\, \epsilon_{\rm mode} \sum_{i=1}^{N_{\rm points}} \mathcal{L}_i \int dE\, G_i(E)\, \sigma_{BW}(E), \qquad (6)$$

where $\mathcal{B}$ denotes branching ratio, $\epsilon_{\rm mode}$ is the overall detection efficiency for the decay mode, i is an index running over the $N_{\rm points}$ energy points, $\mathcal{L}_i$ and G_i are respectively the integrated luminosity and the normalized center of mass energy distribution for each energy point and σ_{BW} is the Breit-Wigner cross section for the reaction $p\bar{p} \to \psi'$.

By taking the ratio of numbers of events for two decay modes, the dependence on much of expression (6) cancels; that ratio is given by the ratio of the $\mathcal{B}$s multiplied by a factor determined only by the overall detection efficiencies for the decay modes considered. It follows that

$$\mathcal{B}(\psi' \to {\rm mode(1)}) = \frac{\epsilon_{\rm mode(2)}}{\epsilon_{\rm mode(1)}} \frac{N_{\rm mode(1)}}{N_{\rm mode(2)}} \mathcal{B}(\psi' \to {\rm mode(2)}) \qquad (7)$$

In particular, for decay mode (1) we obtain

$$\mathcal{B}(\psi' \to e^+e^-) = \frac{\epsilon_{J/\psi\, X}}{\epsilon_{ee}} \frac{N_{ee}}{N_{J/\psi\, X}} \mathcal{B}(\psi' \to J/\psi\, X)\, \mathcal{B}(J/\psi \to e^+e^-) \qquad (8)$$

where $\epsilon_{J/\psi\, X}$ is the overall efficiency (trigger, geometry, detector and analysis) for $J/\psi\, X$ events with the J/ψ decaying to e^+e^-, ϵ_{ee} is the efficiency for e^+e^- events and N_{ee} and $N_{J/\psi\, X}$ are the observed numbers of events. Both $\mathcal{B}(\psi' \to J/\psi\, X)$ and $\mathcal{B}(J/\psi \to e^+e^-)$ are known to higher precision than $\mathcal{B}(\psi' \to e^+e^-)$ [1]; the above formula is used to obtain a better determination of the latter. Reactions (2) and (3) can be written as $\psi' \to J/\psi\, Y \to e^+e^- Y$; the corresponding formula is

$$\mathcal{B}(\psi' \to J/\psi\, Y) = \frac{\epsilon_{J/\psi\, X}}{\epsilon_{J/\psi\, Y}} \frac{N_{J/\psi\, Y}}{N_{J/\psi\, X}} \mathcal{B}(\psi' \to J/\psi\, X) \qquad (9)$$

where $\mathcal{B}(J/\psi \to e^+e^-)$ cancels.

A further advantage of this method is that many of the instrumental and systematic uncertainties cancel in the ratio, including uncertainties in

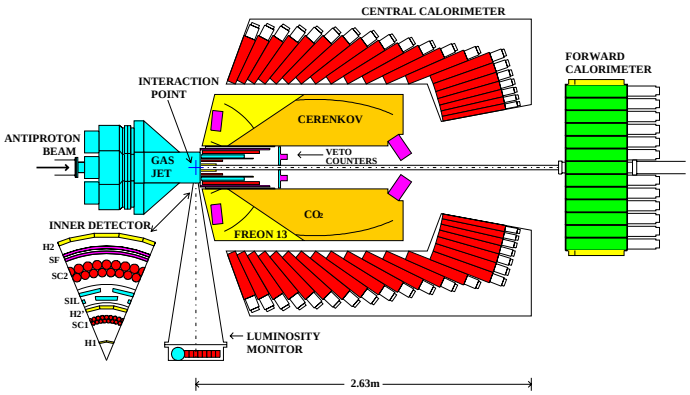

Figure 1: The E835 detector.

the detection efficiency that are common to all decay modes, since all are required to have a well-identified high energy e^+e^- pair. The systematic uncertainties in geometrical acceptance also nearly cancel in the ratio (see section 5).

3 Experimental Apparatus

The E835 experiment is schematically shown in Figure 1. It consists of an internal hydrogen gas-jet target and a non-magnetic spectrometer with cylindrical symmetry around the beam axis, optimized for the detection of electromagnetic final states. The detector sub-systems include: the scintillating counter hodoscopes, the threshold Čerenkov counter, the charged particle tracking system, the electromagnetic calorimeters and the luminosity monitor.

The cooled antiproton beam circulating in the Fermilab Antiproton Accumulator (AA) impinges on the internal gas-jet target [3] of variable density. The gas jet density is incrementally increased during data taking, keeping the instantaneous luminosity approximately constant. Improved pumping and jet alignment systems give better hydrogen confinement in the interac-

tion region ($\simeq 1$ cm^3) than in E760, thus reducing the beam-gas background in the detector by more than a factor 4. The beam is not bunched and the interactions are completely asynchronous.

The hodoscope system includes 3 cylindrical layers of plastic scintillators, (respectively 8 modules 2 mm thick (H1), 24 modules 4 mm thick (H2$'$) and 32 modules 4 mm thick (H2)) that enter the first level trigger for charged events, and provide three dE/dX measurements used in discriminating electrons from gamma conversions. The Forward Veto Counter consists of 8 trapezoidal plastic scintillators normal to the beam axis and is used to reduce the trigger rate by rejecting events with charged tracks in the angular region $3^\circ < \theta < 9^\circ$. Polar angles are defined with respect to the beam direction.

The Čerenkov Counter (Č) [4] enters the first level trigger for electron events and is used off-line for electron identification.

The charged particle tracking system, composed of two Straw Tube Drift Chambers and a Scintillating Fiber Detector sharing a common low-mass mechanical structure and fully contained within a radius of 16 cm, is not used for this analysis. Its total thickness at normal incidence is 0.07 radiation lengths (X_0).

The Central Calorimeter (CCAL) [7] covers the full azimuth angle and $11^\circ < \theta < 70^\circ$ and is composed of 1280 lead glass detectors pointing to the interaction region, arranged in 20 rings in θ and 64 wedges in ϕ. For electromagnetic showers of electrons and gammas, CCAL gives an average resolution of $\sigma_E/E = 0.014 + 0.06/\sqrt{E(GeV)}$ for the energy, 6 mrad for σ_θ and 12 mrad for σ_ϕ, where the angular errors include the uncertainty in the annihilation location. CCAL signals are summed in matrices of 5×8 blocks, forming a coarse θ-ϕ mapping of the whole calorimeter, and then sent to the first level trigger logic to identify high invariant mass events and events with deposited energy exceeding 80% of the total energy [8].

The Forward Calorimeter (FCAL) covers $\theta < 10^\circ$, with a hole for the beam pipe; FCAL data is not used in this analysis.

Luminosity is measured with three silicon detectors mounted at $\theta = 86.5^\circ$ [9]. The luminosity is determined from the recoil proton rate using the well-known elastic scattering cross section.

In order to efficiently utilize the much greater instantaneous luminosity available to E835 compared to E760, the CCAL signals, which are delayed using over 300 feet of coaxial cable, are reshaped so that they are accomodated in 100 ns ADC gates. In addition, TDC read-out was added to nearly all the channels in the detector. This upgrade reduces the background from pile-

up events, allowing the detector to operate at three times the instantaneous luminosity of E760 with the same fraction of contaminated events.

4 Data taking and data analysis

4.1 Data taking

Each data taking cycle (called a "stack") starts with the collection of $\bar{p}$ in the AA; when the beam reaches the desired intensity (between 4×10^{11} and 6×10^{11} stored antiprotons), it is decelerated from the injection momentum to the value appropriate for the resonance under study. The initial jet target density is adjusted to obtain the desired instantaneous luminosity (typically 2.0×10^{31} cm^{-2} s^{-1} which is afterwards kept constant) and data acquisition begins. When enough integrated luminosity is accumulated at a specific energy, the beam is further decelerated, or dumped to start a new stack.

We gathered a total of 10.07 pb^{-1} at a center of mass energy near the ψ' peak, $E_{CM} = 3686$ MeV, in 8 different stacks that were taken at different times during the run with three different triggers (see Tables 1 and 3). Each stack is analyzed separately, to monitor the stability of the detector and possible variations in the results of the analysis.

4.2 Trigger and on-line filter

Interesting events ($\bar{p}p \to (c\bar{c}) \to e^+e^-$ or $\bar{p}p \to (c\bar{c}) \to J/\psi + X \to e^+e^-X$) are characterized by two nearly back-to-back high energy electrons giving a large invariant mass, and a charged track multiplicity of at most 4.

The first level hardware trigger for all (charged) charmonium channels is given by the logical OR of one main trigger condition and two control triggers (see Table 1).

The main trigger, see Table 1, requires at least two "e" signals in coincidence ($2e$), where "e" represents a coincidence of corresponding H1, H2 and Čerenkov detectors, at least two electromagnetic showers in CCAL with large invariant mass ($PBG3$) and a multiplicity cut on the hodoscopes. Initially, (trigger A) the multiplicity cut required at most 4 hits in both H1 (the innermost) and H2 (the outermost) hodoscopes; the condition on H1 multiplicity was soon removed (trigger B) since it did not significantly reduce the trigger rate; after stack 20 the trigger was changed to allow up to 5 hits in

Trigger(stacks)	Branch	
A (2)	Main	$(2e) \otimes \overline{H2 > 4} \otimes \overline{H1 > 4} \otimes PBG3$
B (6,7,8,17)	Main	$(2e) \otimes \overline{H2 > 4} \otimes PBG3$
C (39,40,67)	Main	$(2e) \otimes \overline{H2 > 5} \otimes PBG3$
All Stacks	Control 1	$(1e) \otimes (2h) \otimes (COPL) \otimes (H2 = 2) \otimes PBG3$
	Control 2	$(2e) \otimes (COPL) \otimes (H2 = 2) \otimes \overline{(FCH)}$

Table 1: Triggers for the data used in the analysis.

H2 (trigger C) in order to improve the trigger efficiency for $J/\psi\,\pi^+\,\pi^-$ events which are not reported here. We observe that the trigger is highly efficient for $J/\psi\,\pi^0\,\pi^0$ events in which one or both π^0s decay into one or two Dalitz pairs.

The control triggers given in Table 1 remained stable throughout the data taking. In the first control trigger we require two "h" signals in coincidence $(2h)$ to be back-to-back in azimuth $(COPL)$, where "h" represents a coincidence of corresponding H1 and H2 detectors, and require that just one of the coincidences be associated with the Čerenkov; the second control trigger ignores the calorimeter $(PBG3)$ but requires the hodoscope hits to be back-to-back in azimuth $(COPL)$ and that no charged particle be detected in the forward direction $(\overline{FCH})$.

Event filtering and analysis is done by the online computing systems during data taking, where all events are processed, tagged and written to tape. Events containing at least two electromagnetic showers with invariant mass above 2.2 GeV are written to disk and constitute the data sample for this analysis.

4.3 Event selection

The goal of the offline analysis is the selection of a clean sample of $\psi' \to e^+e^-(X)$ events, and the identification of candidates for each of the decay modes (1)–(3). We first make a preliminary selection and subsequently use kinematical fitting to assign the events to specific event hypotheses.

The preliminary selection requires two electron candidates, each of which has scintillator signals, in at least two of the three hodoscopes, associated with a Čerenkov signal and a CCAL cluster. The invariant mass of the pair must exceed 2.6 GeV. We require that the two electron candidates be within

the fiducial volume of the detector ($15^\circ < \theta < 60^\circ$) for uniform detection efficiency. In order to avoid errors in electron identification and in the energies and angles determined for electrons, we require that the CCAL cluster associated with an electron make an angle of at least 100 mrad with the nearest on-time cluster (electron isolation cut).

We also require electron identification, using dE/dx measurements from H1, H2$'$ and H2, Čerenkov pulse heights and four different CCAL cluster shape variables. These variables are used to build a likelihood ratio for the electron vs. non-electron hypothesis for each electron candidate (EW(i) for the ith electron). The probability distributions for the 8 variables are measured using clean $J/\psi \to e^+e^-$ events for the electron sample and "background" events gathered at center of mass energies away from known resonances for the non-electron sample. Correlation among variables is ignored and EW(i) is taken to be the product of probability ratios for the 8 variables [10]. For each event we require EW(1)$\times$EW(2) > 1.0. The preliminary selection yields 15055 ψ' candidate events. The signal to background ratio in this sample is very high (see Figure 2).

The next step is the assignment of these candidates to the reactions (1)–(3). We first perform a kinematical fit to the $J/\psi\, X$ and e^+e^- hypotheses.

- $\psi' \to e^+e^-$ events are selected by requiring the nominal χ^2 probability[1] of the 4-constraint kinematical fit (P_{ee}) to be greater than 10^{-4}.
- $\psi' \to J/\psi\, X \to e^+e^-X$ events are selected by requiring the nominal χ^2 probability of the 1-constraint kinematical fit to be greater than 10^{-2} and $P_{ee} < 10^{-4}$.

Kinematical fits to the exclusive decay modes, (2) and (3), are then attempted on all events classified as $J/\psi\, X$ and topologically compatible with the hypothesis. $\psi' \to J/\psi\, \pi^0\, \pi^0$ and $\psi' \to J/\psi\, \eta$ events are selected by requiring exactly 6 (4) clusters in the CCAL and the nominal χ^2 probability of the 7C (6C) kinematical fit to be greater than 10^{-6} (10^{-2}). Because of Dalitz decays and photon conversions, events with extra on-time hodoscope signals are rejected only if at least one such hit is unassociated with a Čerenkov signal or unassociated with a π^0 or η decay CCAL cluster.

[1]Since the uncertainties on the energy and direction of a reconstructed track are not normally distributed and correlations between the measurements are not taken into account, the cut on χ^2 probability of kinematical fits cannot be used as a measure of fit efficiency.

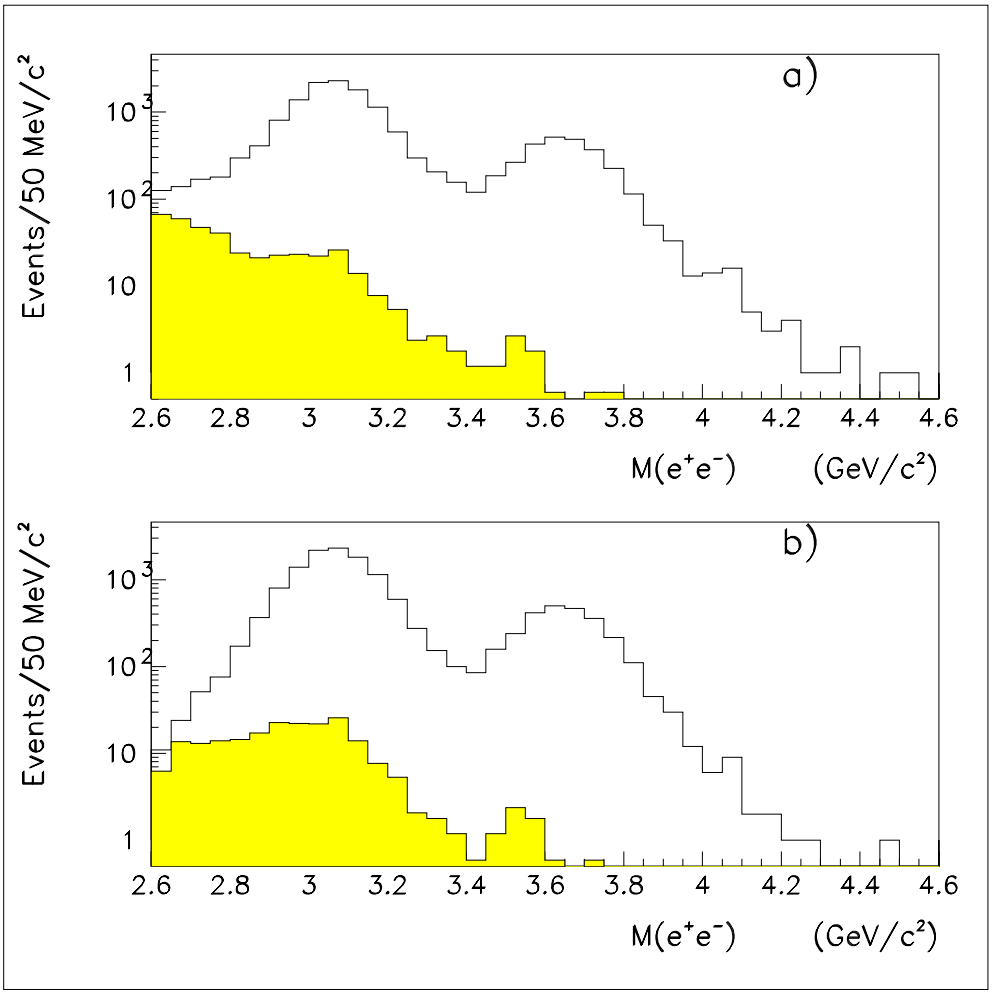

Figure 2: Comparison between signal (unshaded) and non-resonant background (shaded) for all ψ' data. Background has been measured at center of mass energies between 3590 and 3660 MeV and scaled to the integrated luminosity of the signal data. The upper plot is the comparison after the trigger and preliminary selection. The lower plot is the comparison after the event assignment described in the text.

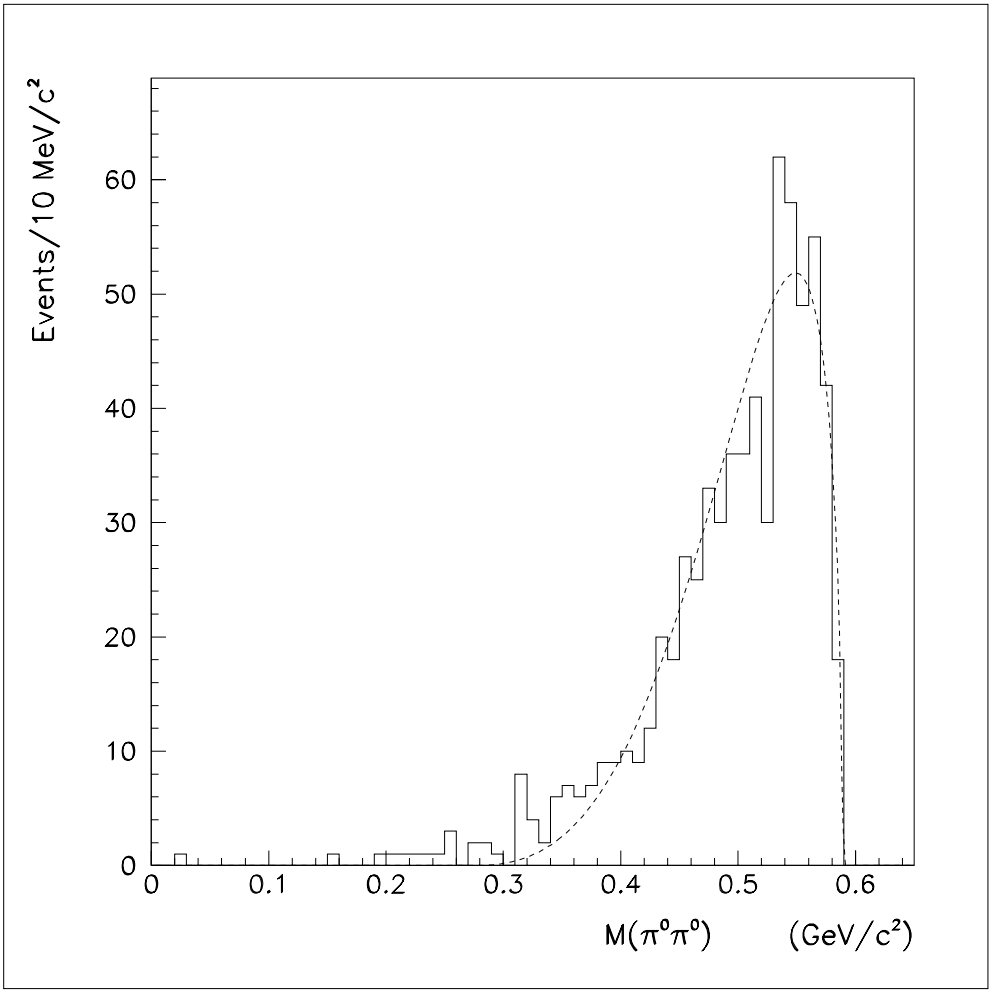

Figure 3: The $\pi\pi$ invariant mass for the $J/\psi\,\pi^0\,\pi^0$ reaction. The dashed curve is calculated assuming S-wave decay and a $J^P = 0^+$ $\pi\pi$ system.

Figure 3 shows the $\pi\pi$ invariant mass distribution for the $J/\psi\,\pi^0\,\pi^0$ reaction. The mass distribution is similar to that observed in ψ' decays by other experiments [2, 11] and its shape is consistent with the hypothesis of S-wave decay to the J/ψ and a $J^P = 0^+$ $\pi\pi$ system.

4.4 Background subtraction

There are two sources of background to the reactions studied: the non-resonant background due to events unrelated to ψ' formation and the internal background due to ψ' events that are not correctly classified.

The non-resonant background is measured by applying the same analysis to data taken, at approximately the same instantaneous luminosity, at E_{CM} between 3590 MeV and 3660 MeV (for 34.2 pb^{-1}). In this sample 1321 events survive the preliminary selection. By normalizing these data to the integrated luminosity of 10.07 pb^{-1} taken at the ψ' resonance, we obtain the estimates of non-resonant background events given in Table 3. The non-resonant background accounts for 390 (2.6%) of the 15055 candidate events. After kinematical fitting and classification the contamination of the sample by non-resonant background is determined to be 1.8% for $J/\psi\,X$, 0.3% for e^+e^-, 0.5% for $J/\psi\,\pi^0\,\pi^0$ and 0.1% for $J/\psi\,\eta$.

The internal background is computed using a full GEANT simulation of the detector. For each ψ' decay mode reported and for all decay modes that contribute to background, 100,000 events were generated, reconstructed and classified according to our criteria. The rest frame angular distributions for $J/\psi \to e^+e^-$ and $\psi' \to e^+e^-$ are of the form $1 + \lambda\cos^2(\theta)$ where θ is the angle between the electron in the ψ (ψ') frame and the beam direction. Reaction (2) is an S-wave decay to J/ψ and a $J^P = 0^+$ $\pi\pi$ system leading to the same value of λ in J/ψ decay as in $\psi' \to e^+e^-$. For reaction (3) λ is different but calculable from the $\psi' \to e^+e^-$ value [12]. For $\psi' \to e^+e^-$ we take $\lambda = 0.69 \pm 0.26$, the value reported by E760 [13]. For ψ' radiative decays we assume pure electric dipole transitions.

The reaction most affected by internal background is $J/\psi\,\eta$, due to contributions from ψ' radiative decay to $\chi_c\,\gamma$ followed by χ_c radiative decay to $J/\psi\,\gamma$ and from $J/\psi\,\pi^0\,\pi^0$ where two photons are out of the calorimeter acceptance or below the 25 MeV threshold. These results are given in Table 2. For consistency with the event selection algorithm, the frequencies given for channels other than e^+e^- are for event samples first classified as $J/\psi\,X$. We observe that for all channels, simulated events are identified correctly as ei-

Generated	Classified as:			
	e^+e^-	$J/\psi\, X$	$J/\psi\,\pi^0\,\pi^0$	$J/\psi\,\eta$
e^+e^-	.9696 $\pm$.0006	.0140 $\pm$.0005		-
$J/\psi\,\pi^0\,\pi^0 \to$ $e^+e^-\gamma\gamma\gamma\gamma$	.0038 $\pm$.0003	.9692 $\pm$.0008	.1877 $\pm$.0034	.0031 $\pm$.0003
$J/\psi\,\pi^+\,\pi^- \to$ $e^+e^-\pi^+\pi^-$ (B)	.0036 $\pm$.0002	.9729 $\pm$.0009	.0028 $\pm$.0003	.0010 $\pm$.0002
$J/\psi\,\pi^+\,\pi^- \to$ $e^+e^-\pi^+\pi^-$ (C)	0.0036 $\pm$0.0002	0.9722 $\pm$0.0009	0.0028 $\pm$0.0003	0.0010 $\pm$0.0002
$J/\psi\,\eta \to$ $e^+e^-\gamma\gamma$	0.0027 $\pm$0.0002	0.9700 $\pm$0.0008	0.0106 $\pm$0.0015	0.3942 $\pm$0.0106
$\chi_{c_1}\,\gamma \to J/\psi\,\gamma\,\gamma$ $\to e^+e^-\gamma\gamma$	0.0010 $\pm$0.0001	0.9721 $\pm$0.0009	0.0075 $\pm$0.0011	0.0146 $\pm$0.0005
$\chi_{c_2}\,\gamma \to J/\psi\,\gamma\,\gamma$ $\to e^+e^-\gamma\gamma$	0.0010 $\pm$0.0001	0.9736 $\pm$0.0005	0.0067 $\pm$0.0007	0.0008 $\pm$0.0001

Table 2: We give the fraction of simulated events classified in each channel, normalized to the number of events passing the trigger and preliminary selection, and, for the exclusive $J/\psi\, X$ channels, to the number classified as $J/\psi\, X$. For each of the decay modes the error quoted refers to the possible stack-dependent effects described in the text. (B) and (C) refer to the triggers given in Table 1.

Stack	$\int \mathcal{L}$ (pb^{-1})	Candidates	e^+e^-	$J/\psi\, X$	$J/\psi\, \pi^0\, \pi^0$	$J/\psi\, \eta$
2	1.01	2831	506	2017	146	36
6	1.44	1635	307	1235	70	19
7	1.09	1831	291	1459	93	25
8	1.10	1616	299	1251	72	18
17	1.34	2008	371	1556	84	24
39+40	2.26	3184	567	2433	142	39
67	1.83	1950	323	1495	84	32
Total	10.07	15055	2664	11446	691	193
Non-resonant Back.		390±10	7.7±1.5	202±8	3.3±1.0	<2
Internal Back.		-	37.1±4.6	39.6±3.8	22.5±3.4	25.9±3.4

Table 3: Candidate events for each decay channel for the ψ' stacks used in this analysis and corresponding background totals.

ther e^+e^- or $J/\psi\, X$ with a frequency of close to 97%, and that systematic uncertainties in identification frequencies vary from 0.06% (e^+e^-) to 2.7% ($J/\psi\, \eta$).

Table 3 gives the numbers of events found for each decay channel in each stack, and the corresponding numbers of internal and non-resonant background events. We find that of the 14665 candidate events after subtraction of non-resonant background, 14110 events, or 96%, are selected as e^+e^- or $J/\psi\, X$, in excellent agreement with the GEANT results described above.

5 Efficiencies and acceptances

Since the number of events observed for each decay mode is compared to the number observed for the $J/\psi\, X$ channel, we require the efficiency and acceptance for each channel relative to that for the inclusive decay $J/\psi\, X$:

$$\frac{\epsilon(J/\psi\, X)}{\epsilon(\mathrm{mode})} = \frac{\epsilon_{\mathrm{tr}}(J/\psi\, X)}{\epsilon_{\mathrm{tr}}(\mathrm{mode})} \frac{\epsilon_{\mathrm{prel}}(J/\psi\, X)}{\epsilon_{\mathrm{prel}}(\mathrm{mode})} \frac{\epsilon_{\mathrm{sel}}(J/\psi\, X)}{\epsilon_{\mathrm{sel}}(\mathrm{mode})}. \tag{10}$$

Here ϵ_{tr} denotes the trigger efficiency (including the fiducial volume acceptance for the electrons), ϵ_{prel} is the efficiency for the preliminary selection, and ϵ_{sel} is the efficiency for the final event selection.

Trigger	λ	e^+e^-	$J/\psi\,\pi^0\,\pi^0$	$J/\psi\,\eta$
A	0.43	0.847±.001	0.896±.001	0.787±.001
	0.69	0.842±.001	0.901±.001	0.718±.001
	0.95	0.839±.001	0.899±.001	0.694±.001
B	0.43	0.852±.001	0.903±.001	0.792±.001
	0.69	0.847±.001	0.907±.001	0.722±.001
	0.95	0.842±.001	0.904±.001	0.697±.001
C	0.43	0.905±.001	0.953±.001	0.839±.001
	0.69	0.901±.001	0.958±.001	0.767±.001
	0.95	0.897±.001	0.956±.001	0.740±.001

Table 4: Trigger efficiency ratios $\epsilon_{\rm tr}(J/\psi\,X)/\epsilon_{\rm tr}(\text{mode})$ for different values of the ψ' decay parameter λ.

5.1 Trigger efficiency

The trigger is designed to select events with two electrons in the angular region $15^\circ < \theta < 60^\circ$. The efficiency of the trigger conditions (see Table 1) is measured with 132 nb^{-1} of data taken at the J/ψ peak energy using a special trigger for which just one electron is required.

We determine the efficiency for detection of a single electron (condition $1e$) to be 0.92 ± 0.01 (systematic error). From this value and the measured efficiencies for the trigger counters, we determine the efficiency of the trigger logic for all of the ψ' decay modes using the simulation described above, taking three possible values for the decay parameter λ. For $\lambda = 0.69$, the fiducial volume acceptance for the $J/\psi\,X$ reaction is 0.51 ± 0.02 and $\epsilon_{\rm tr}(J/\psi\,X)$ is 0.42 ± 0.02 for triggers A and B and 0.45 ± 0.02 for trigger C.

The largest source of systematic error originates from uncertainties in the angular distributions of the reactions. As the J/ψ is almost at rest in the ψ' frame, the laboratory e^+e^- angular distribution is approximately the same for $\psi' \to J/\psi\,X$ and reactions 1 and 2. For reactions 3 and $\psi' \to \chi_c\,\gamma \to J/\psi\,\gamma\,\gamma$ the angular distribution is quite different but these decays contribute less than 5% to $J/\psi\,X$. For a further discussion see [2]. As a consequence, the ratios of trigger efficiencies for e^+e^-, $J/\psi\,\pi^0\,\pi^0$ to $J/\psi\,X$ vary by less than 1% over a wide range of values for λ (see Table 4). The ratio for $J/\psi\,\eta$ varies by 12% over the same range, giving a systematic uncertainty comparable to the statistical uncertainty for this channel.

Decay Mode	e^+e^-	$J/\psi\,\pi^0\,\pi^0$	$J/\psi\,\eta$
$\mathcal{B}(\psi' \to J/\psi\,X)$	0.57 ± 0.04		
$\frac{\epsilon_{\rm tr}(J/\psi\,X)}{\epsilon_{\rm tr}({\rm mode})}$	0.868 ± 0.005	$0.927\pm^{0.000}_{0.005}$	$0.740\pm^{0.070}_{0.025}$
$\frac{\epsilon_{\rm prel}(J/\psi\,X)}{\epsilon_{\rm prel}({\rm mode})}$	$1.074\pm.004$	$1.129\pm.003$	$1.019\pm.003$
$\frac{\epsilon_{\rm sel}(J/\psi\,X)}{\epsilon_{\rm sel}({\rm mode})}$	1.003 ± 0.001	5.35 ± 0.13	2.56 ± 0.10

Table 5: Sources of systematic error, including the branching ratio for $J/\psi\,X$ and the stack averaged trigger, preliminary selection and event selection efficiency ratios. The preliminary selection and event selection efficiencies for the $J/\psi\,X$ channel are 0.67 ± 0.01 and 0.97 ± 0.01 respectively.

5.2 Preliminary selection efficiency

The preliminary selection includes the requirement that a Čerenkov signal and hodoscope hits be found for each electron, the EW cut, the electron isolation cut and the invariant mass cut. The efficiency for this selection is computed by Monte Carlo simulation. Separate elements of the efficiency are checked against data as described below.

The efficiency for finding both electron candidates associated with Čerenkov and hodoscopes is evaluated by simulation and found to be independent of decay mode and of instantaneous luminosity. The result is $\epsilon_{\check{C}}^{MC} = 0.982 \pm 0.002$, where the systematic error arises from uncertainties in the geometry and light collection of the detector. It is in excellent agreement with the Čerenkov efficiency measured using clean event samples of $J/\psi \longrightarrow e^+e^-$, $\chi_2 \longrightarrow J/\psi\,\gamma$ and $\psi' \to e^+e^-$, giving $\epsilon_{\check{C}}^{\rm data} = 0.981 \pm 0.001$, which we find to be stable in time with no significant center of mass energy dependence. Its value does not affect the branching ratios because it cancels in Eqs. 8 and 9.

The efficiency of the electron identification cut (EW) is measured to be 0.92 ± 0.01 using clean event samples of $J/\psi \longrightarrow e^+e^-$, $\chi_2 \longrightarrow J/\psi\,\gamma$ and $\psi' \to e^+e^-$. This efficiency depends weakly on the angle between the electron shower and the closest cluster in CCAL. For angles greater than 100 mrad however, the EW efficiency does not depend on the specific final state, and it too cancels in Eqs. 8 and 9.

The efficiency of the electron isolation cut depends on the number of final state particles for each specific decay mode and is computed by simulation.

Since the e^+e^- invariant mass is larger in the e^+e^- decay mode than for

the $J/\psi\, X$ modes, the cut ($M_{e^+e^-} > 2.6$ GeV) produces a larger inefficiency for the latter modes. By simulation, we determine $\epsilon_{M_{ee}}(J/\psi\, X)/\epsilon_{M_{ee}}(e^+e^-) = 0.992 \pm 0.002$, where the systematic error originates in the accuracy of simulation for the calorimeter energy resolution.

There are stack-dependent systematic errors in the preliminary selection efficiency due primarily to noisy detector channels and luminosity-dependent accidental low energy clusters in CCAL. These effects are studied by using real events acquired throughout data taking by a random trigger, given by a pulser asynchronous with respect to physics triggers. These events are superimposed on Monte Carlo events at the appropriate rate and the effect included in the computed efficiency.

The preliminary selection efficiency ratios are shown in Table 5 which summarizes the sources of systematic error.

5.3 Event selection efficiency

The kinematical fit and topological cut efficiencies (including π^0 and η acceptances), are calculated by simulation. The run-dependent effects described above are taken into account using random triggers to add noise and accidental CCAL clusters. These effects particularly affect the $J/\psi\,\pi^0\,\pi^0$ and $J/\psi\,\eta$ decay modes since their selection requires exactly 6 (4) in-time clusters in CCAL. Selection efficiency ratios are also shown in Table 5.

6 Results

We give the ratios of signal events, overall efficiencies and branching ratios in Table 6, where each trigger condition is analyzed separately. From equations 8 and 9, averaging over all stacks and using the PDG96 [14] "Our Fit"[2] value of 0.57 ± 0.04 for $\mathcal{B}(\psi' \to J/\psi\, X)$ (determined by a constrained fit to 7 ψ' branching ratios using 13 measurements) and the PDG98 [1] values of the $J/\psi \to e^+e^-$ and $\eta \to \gamma\gamma$ branching ratios, we obtain the results listed in Table 7. Systematic errors are combined in quadrature. We also give the values reported by the Particle Data Group (PDG96) [14] and the measurements of E760 [2].

[2]We do not use the PDG98 "Our Fit" result for $\mathcal{B}(\psi' \to J/\psi\, X)$ because a measurement of $\psi' \to \mu^+\mu^-$ was mistaken for one of $\psi' \to J/\psi\,\mu^+\,\mu^-$ and included in the PDG fit procedure.

Channel	Stack#	$\frac{N(\text{mode})}{N(J/\psi X)}$	$\frac{\epsilon(J/\psi X)}{\epsilon(\text{mode})}$	$\frac{\mathcal{B}(\text{mode})}{\mathcal{B}(J/\psi X)\mathcal{B}(J/\psi \to e^+e^-)}$
$\psi' \to e^+e^-$	2	.251±.013	.907±.006	.228±.012±.001
	6,7,8,17	.234±.007	.913±.006	.214±.007±.001
	39,40,67	.227±.009	.971±.006	.220±.009±.001
	Average			.216±.005±.001
Channel	Stack#	$\frac{N(\text{mode})}{N(J/\psi X)}$	$\frac{\epsilon(J/\psi X)}{\epsilon(\text{mode})}$	$\frac{\mathcal{B}(\text{mode})}{\mathcal{B}(J/\psi X)}$
$\psi' \to J/\psi\,\pi^0\,\pi^0$	2	.0713±.0063	5.44±.13	.388±.034±.009
	6,7,8,17	.0570±.0035	5.48±.13	.312±.016±.007
	39,40,67	.0565±.0035	5.79±.14	.327±.020±.008
	Average			.328±.013±.008
Channel	Stack#	$\frac{N(\text{mode})}{N(J/\psi X)}$	$\frac{\epsilon(J/\psi X)}{\epsilon(\text{mode})}$	$\frac{\mathcal{B}(\text{mode})\mathcal{B}(\eta \to \gamma\gamma)}{\mathcal{B}(J/\psi X)}$
$\psi' \to J/\psi\,\eta$	2	.0159±.0031	1.87±.19	.0297±.0058±.0030
	6,7,8,17	.0137±.0017	1.88±.19	.0258±.0032±.0026
	39,40,67	.0167±.0023	2.00±.20	.0334±.0046±.0033
	Average			.0282±.0024±.0028

Table 6: Ratios of signal event totals, overall efficiencies and branching ratios. The errors in columns 3, 4 and 5 are respectively statistical, systematic and statistical/systematic.

Channel	E835	E760	PDG 96
$\mathcal{B}(\psi' \to e^+e^-)$	$(7.4 \pm 0.2 \pm 0.7) \times 10^{-3}$	$(8.3 \pm 0.5 \pm 0.7) \times 10^{-3}$	$(8.8 \pm 1.3) \times 10^{-3}$
$\mathcal{B}(\psi' \to J/\psi\,\pi^0\,\pi^0)$	$(18.7 \pm 0.9 \pm 1.3)\%$	$(18.4 \pm 1.9 \pm 1.3)\%$	$(18.4 \pm 2.7)\%$
$\mathcal{B}(\psi' \to J/\psi\,\eta)$	$(4.1 \pm 0.3 \pm 0.5)\%$	$(3.2 \pm 1.0 \pm 0.2)\%$	$(2.7 \pm 0.4)\%$

Table 7: Results of this analysis compared with E760 results and PDG96 world averages. Errors are statistical/systematic.

For the $\psi' \to e^+e^-$ branching ratio, the value $(7.4 \pm 0.2(\text{stat.}) \pm 0.7(\text{syst.})) \times 10^{-3}$ is an improvement over the E760 result by a factor 3 in the statistical error. The systematic error is dominated by uncertainty in the $J/\psi\,X$ branching ratio. A future improved measurement of the latter and of the $J/\psi \to e^+e^-$ branching ratio will enable a better determination.

Our results for the branching ratios for $\psi' \to J/\psi\,\pi^0\pi^0$ and $\psi' \to J/\psi\,\eta$ are also better than the E760 results with regard to statistical error. The dominant systematic uncertainty for the former is from the $J/\psi\,X$ branching ratio and will be reduced by a future improved measurement. For the latter, we have roughly comparable systematic uncertainties from the $J/\psi\,X$ branching ratio and the decay angular distribution.

7 Acknowledgments

The authors wish to thank the staffs, engineers and technicians at our respective institutions for their valuable help and cooperation. This research was supported by the U.S. Department of Energy and the Italian Istituto Nazionale di Fisica Nucleare.

References

[1] C. Caso *et al.*, Review of Particle Physics, Eur. Phys. J. **C 3**, 1 (1998).

[2] T. Armstrong *et al.*, Phys. Rev. **D 55**, 1153 (1997).

[3] D. Allspach *et al.*, Nucl. Instr. & Meth. A410, 195-205 (1998).

[4] S. Bagnasco *et al.*, Nucl. Instr. & Meth. A424, 304-20 (1999).

[5] S. Bagnasco *et al.*, Nucl. Instr. & Meth. A409, 75-8 (1998).

[6] M. Ambrogiani *et al.*, Nucl. Instr. & Meth. A419, 632 (1998).

[7] L. Bartoszek *et al.*, Nucl. Instr. & Meth. A301, 47 (1991).

[8] R. Ray *et al.*, Nucl. Instr. & Meth. A307, 254-264 (1991).

[9] S. Trokenheim *et al.*, Nucl. Inst. & A355, 308 (1995).

[10] M. Ambrogiani *et al.*, Phys. Rev. **D 60**, 03002/1-6 (1998).

[11] R. Brandelik *et al.*, Z. Phys. **C 1**, 233 (1979). W. Tanenbaum *et al.*, Phys. Rev. **D 17**, 1731 (1978).

[12] A. J. Smith, Ph.D. thesis, University of California, Irvine, 1993 (unpublished).

[13] T. Armstrong *et al.*, Phys. Rev. **D 47**, 772 (1993).

[14] R. M. Barnett *et al.*, Phys. Rev. **D 54**, 1 (1996).